ROTATION AND MASS OF THE LARGE MAGELLANIC CLOUD

Gerard de Vaucouleurs
Harvard College Observatory
Received May 11, 1959; revised October 2, 1959

ABSTRACT

New optical velocities of outlying nebulosities observed with the Mount Stromlo 74-inch reflector are used in conjunction with the old Lick velocities for a rediscussion of the rotation-curve and a revision of the mass estimate previously derived from the Sydney radio observations

If $m_0 - M = 19.0$ and $i = 63°$, the maximum rotational velocity is $V_r \simeq 145$ km/sec at $r \simeq 3.5$ kpc, and the revised mass is $\mathfrak{M} = (2.5 \pm 0.6 \text{ p.e.}) \times 10^{10}$ ⊙; the absorption-free mass-luminosity ratio $\mathfrak{M}/\mathfrak{L}_0$ is about 6, and the ratio of neutral hydrogen to total mass H I/$\mathfrak{M}$ is 4–5 per cent

The evidence for spiral structure in the Large Cloud is reviewed in Appendix I. A possible interpretation for the discrepancy between radio and optical rotation-velocities is outlined in Appendix II; it appears plausible that the radio estimate of the mass may be too low by a factor ×3 and the optical estimate too high by a factor ×2.

I. INTRODUCTION

The rotation of the Large Magellanic Cloud was first suggested by Wilson (1918) as a possible interpretation of his measures of the velocities of 17 emission nebulosities (1918) (an eighteenth object is listed by Voute 1926); the interpretation in terms of a large transverse motion, advanced as an alternative by Hertzsprung (1920, 1923), was generally accepted during the next three decades (Luyten 1928; Wilson 1944). In a paper which seems to have passed unnoticed Kaburaki (1931) analyzed the Lick velocities and showed rather convincingly that, even if a large transverse motion is assumed, the residual velocities "suggest the occurrence of rotation" around an axis defined by points A ($4^h52^m.0$, $-69°23'$) and B ($5^h26^m.2$, $-68°14'$) (1900). However, he made no attempt to determine the center of rotation or the tilt of the equatorial plane, and the various estimates of the rotation period range from 5×10^7 to 8.5×10^8 years for an assumed distance of 34.5 kpc.

Unaware of this paper, which has come to his attention only recently, the writer advocated anew the rotational interpretation after photographic observations had detected extensive spiral structure in the faint outer regions of the system (de Vaucouleurs 1954*a*, *b*, 1955*a*).[1] This rotational interpretation was finally placed beyond doubt through a detailed analysis of radio observations of the 21-cm-line emission (Kerr, Hindman, and Robinson 1954; Kerr and de Vaucouleurs 1955, 1956) and a discussion of the optical velocities of 26 supergiant stars (Feast, Thackeray, and Wesselink 1955).

The mass derived from the 21-cm observations was 3×10^9 solar masses, for an estimated tilt angle $i = 65°$ and an assumed distance $\Delta = 46$ kpc. However, apart from the uncertainty in i and Δ and the exploratory nature of the observations, the interpretation of the radio data is subject to a fundamental uncertainty arising from the complex structure of the 21-cm-line profiles and the attendant choice of the component most likely to arise in the equatorial plane of the system. To assist in the interpretation of future improved radio observations, additional optical velocities of emission nebulosities were necessary. The small z-component of the optical-velocity dispersion of these objects in the Large Cloud, about 5 km/sec (de Vaucouleurs 1955*c*), is good indirect evidence of their concentration in or close to the equatorial plane. There is also ample direct evidence for this location in Magellanic systems seen edgewise and, of course, in all regular spirals.

[1] See Appendix I.

II. OBSERVATIONS

In order to supplement the Lick data, seven bright emission nebulosities were chosen from the catalogue of Henize (1956) among the most distant from the center of the bar and located north and south of it near the major axis. The positions of these objects and of the eighteen observed by Wilson are plotted in Figure 1 on an outline map of the Cloud.

All observations were taken at the Newtonian focus of the 74-inch reflector with the medium (B) dispersion of the Zeiss spectrograph giving a dispersion of 150 A/mm at Hγ; with a slit width of 80 μ = 1$''$.8 and a slit/image ratio = 2.7, the two components of [O II] 3726–29 are clearly resolved on the plates. For all other instrumental details and an account of reduction procedures, see G. and A. de Vaucouleurs (1960). The measured velocities are listed in Table 1, where the successive columns give (1) the identification in Henize's catalogue, (2, 3) R.A. and $-D$ (1950), (4) date, (5) exposure time (103*a*-O emulsion in all cases), (6, 7, 8) length, width, and position angle of slit, (9) number of emission lines measured, (10) the average deviation of individual lines from the mean velocity, (11) the observed mean velocity (the reduction to the sun is negligible, since the south pole of the ecliptic is within the borders of the Cloud), (12) the estimated probable error of the mean (the large p.e.'s of N 11 B and N 11 C, measured differentially against 30 Doradus with a long slit, are due to uncertainty in the curvature correction), (13) NGC number, if any, and remarks.

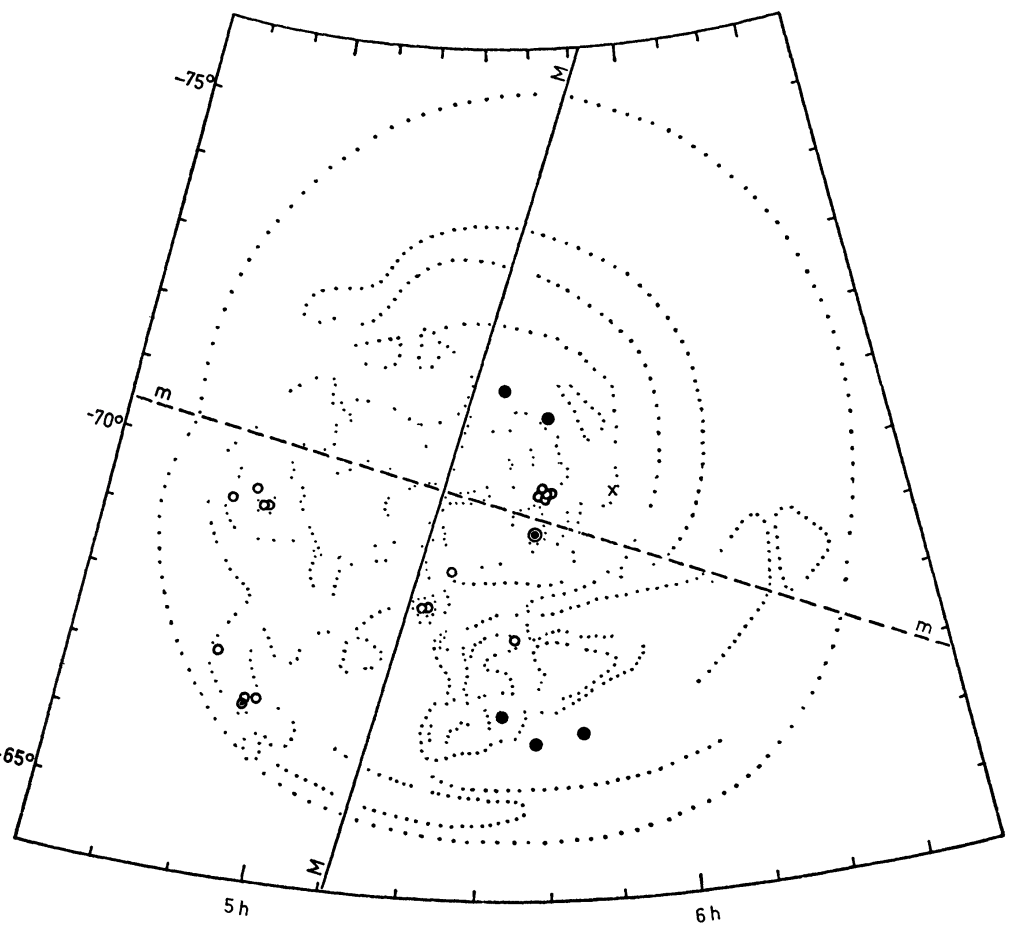

FIG. 1.—Outline map of Large Magellanic Cloud, showing location of emission nebulosities whose radial velocities are known. *Circles and cross:* Lick data; *dots:* Mount Stromlo data.

A check of the over-all systematic accuracy is provided by the mean observed velocity, $V = +270 \pm 7$ (p.e.) km/sec of the 30 Doradus nebula (NGC 2070) and central star; the Lick velocity of NGC 2070 is $+275 \pm 6$, the mean velocity of the group (No. 4) of 6 nebulosities associated with it is $+261 \pm 3$ (+263, after Wilson); the corresponding median velocity in the radio observations (Kerr and de Vaucouleurs 1955, p. 517) is $+272 \pm 3$ (p.e.). It is clear that the Mount Stromlo and the Lick velocities are directly comparable, and any systematic error is well within the accidental errors of either set.

TABLE 1

RADIAL VELOCITIES OF EMISSION NEBULOSITIES IN THE LARGE MAGELLANIC CLOUD

No (1)	R A (2)	$-D$ (3)	Date 1956–1957 (4)	Expos (min) (5)	Slit l(mm) (6)	Slit $w(\mu)$ (7)	p a (8)	Lines (9)	A D (km/sec) (10)	V (km/sec) (11)	p e (km/sec) (12)	Notes (13)
30 Dor . .	5^h38^m9	69°06′	Nov. 25	6	2 0	80	90°	4	26	+273	13	1
NGC 2070	. .	. .	Dec. 23	4	2 0	80	90°	9	28	+269	8	2
N 11-B	4 56 8	66 28	Dec. 25	60	10 0	60	124°	7	35	+330:	25:	3
N 11-C	4 57 7	66 32	Dec. 26	120	10 0	60	14°	5	26	+399?	25:	4
N 55-A	5 32 5	66 29	Dec. 24	90	3 0	80	0°	9	26	+323	8	
N 63-A	5 35 7	66 02	Dec. 24	90	2 0	80	0°	8	25	+312	8	. . .
N 72	5 43 6	66 17	Dec. 23	130	2 0	80	90°	9	31	+334	10	5
N 206-A	5 32 0	71 06	Jan 30	225	2 0	80	0°	9	25	+218	8	.
N 213-A	5 38 9	70 42	Dec 27	135	2 0	80	90°	12	18	+185	6	6

NOTES TO TABLE 1

1. Central star.
2. Lick: +275; bright arch.
3. Lick: +296; NGC 1763, 30 Dor Std, long slit, curvature correction uncertain.
4. NGC 1769, 30 Dor Std, long slit, curvature correction uncertain.
5 Measured twice.
6. NGC 2075.

III. ROTATION

In order to derive rotational velocities from the observed radial velocities, we must determine (1) the co-ordinates of the center of rotation, (2) the position angle of the major axis, (3) the tilt angle of the equatorial plane to the line of sight, (4) the correction for solar motion (galactic rotation and translation), and (5) the systemic velocity at the center of rotation.

The determination of these elements is a little more complicated or uncertain for the Large Cloud than for more regular and more distant spirals.

a) Center of Rotation

In the 1956 discussion of the radio observations the velocities were plotted for two centers: (1) the optical center, C, at 05^h24^m, $-69\overset{\circ}{.}8$, which led to a strongly asymmetric velocity-curve, and (2) the radio center, C_r, at 05^h20^m, $-68\overset{\circ}{.}8$, defined by the condition that the resultant velocity-curve be symmetric (Kerr and de Vaucouleurs 1956, p. 512). The second center was adopted for two reasons: (1) the center of gravity of the surface density distributions of light, stars, and hydrogen emission is shifted from C in the general direction of C_r, and it was felt that this might indicate the location of the overall center of gravity of the system governing the rotational motion of the outer regions of the H I envelope; (2) all available models for the derivation of the total mass of a rotating galaxy assume that the velocity-curve is symmetrical about the center of rotation.

In a discussion of optical velocities, which all refer to the bright central area within 4° from either center, it is plausible that the center should be determined by the optical structure of this region, in which, as shown previously (de Vaucouleurs 1955*a*, 1957*a*), the inner isophotes locate accurately the center of symmetry of the bar in C, at 05^h24^m, $-69\overset{\circ}{.}8$ (1950), and by the optical and/or radio velocity distribution in this same region. Figure 2 is a map of the radio median velocities showing contours of equal velocity residual, i.e., the observed velocity corrected for standard solar motion and galactic rotation (see Kerr and de Vaucouleurs 1955, Pl. I, where individual values are plotted); the center of symmetry of the pattern is C_0 at 05^h25^m, $-70\overset{\circ}{.}0$, within $0\overset{\circ}{.}25$ from C, which is therefore adopted as the center of rotation for the present discussion of optical velocities.

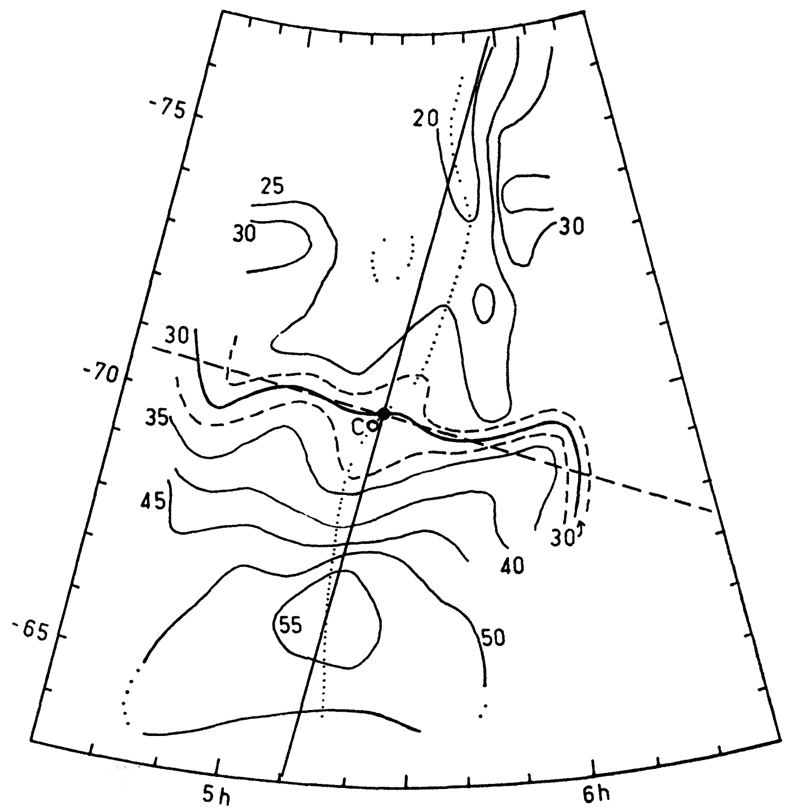

FIG 2.—Contour map of radio median residual velocities, showing location of symmetry axes of the velocity distribution.

b) *Major Axis*

Figure 2 also locates accurately the long axis of symmetry of the velocity distribution through C_0 and the velocity maxima and minima in position angle 166°; the minor axis defined by $V(C_0) = 30$ km/sec is precisely orthogonal to the major axis. This and previous determinations are collected in Table 2. The agreement of three independent methods and sets of data leaves little room for uncertainty here.

c) *Tilt Angle*

In the discussion of the radio velocities a provisional estimate, $i = 65° \pm 5°$, was adopted. A later, more accurate determination, $i = 63° \pm 3°$: (p.e.), was obtained from the axial ratio $b/a = 0.89 \pm 0.01$ (p.e.) of the outer isophotes in red light (de Vaucouleurs 1957*a*). Exactly the same value is indicated in blue light (Elsässer 1959). This value will be accepted here without modification. The p.e. attached to i makes some allowance for possible small departures from true circularity of the outer loop in its own plane; however, since the position angle of the major axis of the corresponding isophotes agrees so closely with the position angle of maximum velocity gradient (Table 2), it is clear that any departure must be small, unless the loop should chance to be elongated precisely in this direction or at right angles to it.[2]

Since the rotational velocity is proportional to sec i and the mass to $\sec^2 i$, obviously a serious uncertainty enters here; to the probable error of $\pm 3°$ in i corresponds, for sec i, a range 2.00–2.46 and, for $\sec^2 i$, a range 4.0–6.0; the values $\sec i = 2.2 \pm 0.2$: and $\sec^2 i = 5.0 \pm 1.0$: (p.e.) will be used. An analysis of a large number of accurate optical or radio velocities may eventually reduce this fundamental uncertainty due to the unfavorable presentation of the system.

TABLE 2

POSITION ANGLE OF MAJOR AXIS OF THE LARGE CLOUD

Method	Position Angle	Remarks
Optical velocities	165° 161°	1 2
Radio velocities.	170° 166°	3 4
Optical isophotes	160° 170°	5 6
Adopted mean position angle	165°±1° (p.e)	

NOTES TO TABLE 2

1 Maximum gradient of stellar velocities (Feast *et al.* 1955).
2 A redetermination of symmetry axis of curve in Fig. 1 of Feast *et al.* (1955).
3 Maximum gradient of radio median velocities (Kerr and de Vaucouleurs 1955).
4 A redetermination of symmetry axis in Fig 2.
5 Major axis of outer spiral arm and star density contours (de Vaucouleurs 1955*a*, p. 137).
6. Major axis of outer isophotes (de Vaucouleurs 1957*a*, p. 78).

d) Solar Motion

In the reduction of the radio data the observed velocities were corrected for a local solar motion of 20 km/sec toward 18^h, $+30°$, and for a galactic rotation of 270 km/sec toward $l = 57°$, $b = 0°$. The correction at the Cloud rotation center, C, then is -243 km/sec. In the present discussion the correction for a total solar motion of 300 km/sec toward $l = 55°$, $b = 0°$, with respect to the Local Group of galaxies (Humason and Wahlquist 1955) will be applied. This is the "standard" treatment for the reduction of velocities of external galaxies to the galactic center; for the Large Cloud area the correction is $-297 \cos b$ km/sec, and at the rotation center ($b = -33.°0$) it is -249 km/sec.

[2] The fact that it is difficult to determine i precisely does not justify the assumption recently propounded by some astronomers that $i \simeq 0°$, which reduces the mass derived from the radio observations to one-third of that (3×10^9 ☉) quoted above. The hypothesis that the Cloud is seen edgewise implies that the system is almost spherical, since it is nearly circular in outline; this would require that the conspicuous bright bar be oriented either along the rotation axis or possibly along the line of maximum velocity gradient, while it is actually tilted at about 45° to either of them (see Figs. 1 and 2). Further, this assumption is flatly contradicted by the presence of the nearly circular outer Loop of the Cloud (see Fig. 1 and Appendix I) and by the strong flattening of systems of the same type when seen edgewise, such as NGC 55 (Kerr and de Vaucouleurs 1955), NGC 4631, etc.

Which treatment applies best to the Magellanic Clouds, which may or may not share the motion of translation of the Galaxy in the Local Group, is debatable; however, a change ΔV_G in the galactic rotation vector causes a change of only 0.82 ΔV_G in the systemic velocity and none in the rotational-velocity component for points near the major axis, which is parallel to the galactic plane (see Kerr and de Vaucouleurs 1955, p. 510).

e) Systemic Velocity

The radio median velocity at the optical rotation center C is $+273 - 249 = +24$ km/sec; the optical velocity of 30 Doradus (mean of Lick and Mount Stromlo, Table 3), which is very close to the minor axis, is $+273 - 254 = +19$ km/sec; that of nearby group IV (5 nebulae), $+255 - 254 = +1$ km/sec. Group I (3 nebulae), which is a little more distant from the minor axis and on the opposite side of C, is $+261 - 243 = +18$ km/sec. Three trial values, $V_s = 0, +10$, and $+20$ km/sec have been used; the adopted value $V_s = +10 \pm 3$ (p.e.) was determined by the condition that the average deviation of the rotational velocities from the mean relation $V_r = kr$ be a minimum. The term k was determined by the objects (A) closest to the major axis (groups II, III, V, VI), while the objects (B) closest to the minor axis (groups I, IV, and 30 Dor) are most sensitive to error in V_s. The (unweighted) average deviations are given in the accompanying table.

V_s	0	+10 (km/sec)	+20 (km/sec)
k .	50 4	44 8	39 2 km/sec per degree
(A)	37	43	52 A D (km/sec)
(B) .	109	65	107 A D. (km/sec)
(A+B). .	68	53	75 A.D (km/sec)

f) Rotation Velocities

Let r_0, θ_0, V_0 be the observed polar co-ordinates and velocity. The corresponding co-ordinates r and θ in the plane of the system and the rotational velocity V_r are given by the following relations (see Kerr and de Vaucouleurs 1955):

$$\tan\theta = \tan\theta_0 \operatorname{cosec} i\,, \tag{1}$$

$$r = \frac{r_0 \sec\theta}{\sec\theta_0}\,, \tag{2}$$

$$V_r = \frac{V_0 - V_s}{\cos\theta \cos i} = (V_0 - V_s)\, f\,. \tag{3}$$

The values of $V_0 - V_s$, θ, r, V_r, and f are listed in Table 3 for all objects observed at either Lick or Mount Stromlo. The weights w and adopted velocities of the Lick data are slightly revised (de Vaucouleurs 1955*c*); unit weight corresponds to p.e. = ± 10 km/sec; velocities from single spectra of $w = \frac{1}{4}$ (Lick: IC 2105, NGC 2111, weight unknown; Mount Stromlo: N 11-B, N 11-C) were rejected. In the determination of the rotation-curve, the weight of V_r was taken as $W = w/f$. The individual values (*dots*, $W > 0.5$; *crosses*, $W < 0.5$) and mean points (*circles*) are plotted in Figure 3; the dotted interpolation curve, according to Bottlinger's formula, is

$$V^2 = \frac{a\, r^2}{1 + b\, r^3}\,, \tag{4}$$

where $a = 3.3 \times 10^3$ (km/sec)^2 (deg)$^{-2}$, and $b = 0.024$ (deg)$^{-3}$; the continuous curve refers to the model of Section IV.

The maximum slope ($r < 1°$) is 57 km/sec per degree; the mean slope of the quasi-straight part ($r \leqslant 2°$) is 54 km/sec per degree; the maximum rotational velocity is about 145 ± 10 (p.e.) km/sec, near $r \simeq 4°5$ according to Bottlinger's formula, near 3°5 ± 0°1: (p.e.) according to the model. The corresponding value for the radio data was about 70 km/sec near $r \simeq 3°2$. It will be observed in Figure 3 that points which depart strongly from the rotation-curve are of low weight (*crosses*, $W < 0.5$) and generally represent objects close to the minor axis which have only small rotational-velocity components in

TABLE 3

ROTATIONAL VELOCITIES OF EMISSION NEBULOSITIES IN THE LARGE MAGELLANIC CLOUD*

Group	No.	V	w	θ	r	f	$V_0 - V_s$	V_r	w/f
I	NGC 1722	+265	2 75	75°7	+2°91	8 92	+12	+107:	0 31
	1743	+260	2 5	70 7	+2 79	6 68	+ 7	+ 47:	0 37
	1748	+256	2 0	71 1	+2 72	6 82	+ 3	+ 20:	0 29
II	1714	+309	3 0	40 7	+4 09	2 91	+58	+169	1 03
	1763	+296	2 0	28 7	+4 13	2 51	+45	+113	0 80
	IC 2115	+292	2 25	28 2	+4 17	2 50	+41	+103	0 90
III. .	NGC 1935	+299	2 5	8 9	+1 70	2 23	+39	+ 87	1 12
	1936	+292	2 5	11 2	+1 75	2 25	+32	+ 72	1 11
	1949	+260	0 5	24 8	+1 23	2 43	0	0	0 21
	2029	+297	0 75	36 0	+2 34	2 72	+37	+101	0 28
IV ..	2077	+255	1 5	78 3	−1 51	10 9:	− 9	− 98:	0 14
	2079	+255	2 0	73 8	−1 57	7 95	− 9	− 72:	0 25
	2080	+251	5 0	78 3	−1 57	10 9:	−13	−142:	0 46
	2086	+271	2 25	77 9	−1 68	10 5:	+ 7	+ 74:	0 21
	Anon	+264	0 5	77 9	−1 60	10 5:	0	0:	0 05
IV*a*	NGC 2070	+273	5 5	81 5	+1 65	14 9:	+ 9	+134:	0 37
V. ..	N 55-A	+323	1 5	34 5	+3 46	2 67	+59	+158	0 56
	N 63-A	+312	1 5	40 7	+3 94	2 90	+48	+140	0 52
	N 72	+334	1 0	50 2	+4 24	3 43	+70	+240	0 29
VI .	N 206-A	+218	1 5	17 2	−1 65	2 30	−46	−106	0 65
	N 213-A	+185	2 75	41 2	−1 89	2 94	−79	−231	0 93

* Groups I–IV: Lick; IV*a*: Lick and Mt Stromlo; V, VI: Mt Stromlo r negative for objects south of minor axis; $V_s = +10$ km/sec; $i = 63°$; $w = 1$ for p e = 10 km/sec; V: observed velocity, V_0: velocity corrected for solar motion, V_r rotational velocity

ROTATION CURVE: MEAN POINTS

Range of $\lvert r \rvert$	$\langle \lvert r \rvert \rangle$	$\langle \lvert V_r \rvert \rangle \pm$ p e	$\Sigma w/f$
1 23–1 75	1°63	82 5	4 58
1 89–3 46 ..	2 58	141 5	2 74
3 94–4 24.	4 11	141	3 54
1 23–2 91 . .	1 86	100 ±10	6 76
3 46–4 24..	4 02	144 ±10	4 10

the line of sight; any observational error or random velocity in these points is therefore greatly magnified in Figure 3. All other points, but one, of weight $W > 0.5$ (*dots*) representing objects nearer the major axis are much more closely grouped near the adopted rotation-curve. The exception is N 213-A, which leaves a residual of +130 km/sec in V_r or 60 km/sec in $V_0 - V_s$; there is no obvious reason for this in the observations; the velocity derived from 12 lines on a well-exposed spectrogram has the smallest internal probable error.

The average deviation (for unit weight $W = w/f = 1$) from the interpolation curve is 34 km/sec for 12 points near the major axis of mean weight 0.70, and 61 km/sec for 9 points near the minor axis of mean weight 0.27; it is 42 km/sec for all 21 points of mean weight 0.51.

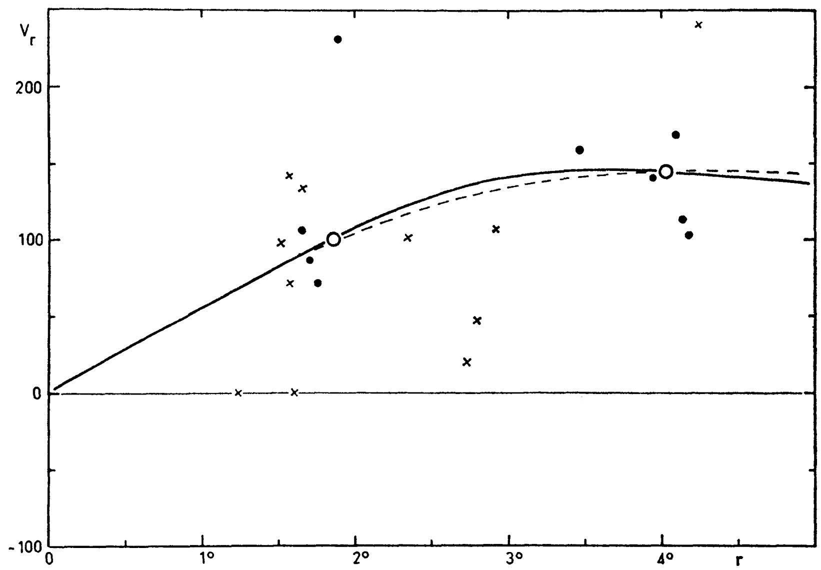

FIG. 3.—Rotation-curve of Large Magellanic Cloud from optical velocities of emission nebulosities. *Crosses:* low-weight points ($W < 0.5$), referring mainly to objects near minor axis. *Dots:* high-weight points ($W > 0.5$), referring to objects close to major axis. *Circles:* mean points. *Dashed curve:* Bottlinger's interpolation formula. *Full curve:* adopted composite spheroid model

A small part of this scatter arises from the observational errors (p.e. = ±10 km/sec) and the cosmic dispersion ($\sigma = \pm 7$ km/sec; see de Vaucouleurs 1955*c*); the p.e. arising from all other causes is about ±25 km/sec for points near the major axis.

The period of rotation is $P = 2\pi r/V_r = 6.16 \times 10^9/\omega$ (years) if ω is in km/sec/kpc; the variation of P as a function of r according to the composite spheroid model of Section IV is shown in Figure 5. In the central regions, $P \simeq 1.2 \times 10^8$ years; at the edge of the main body, near $r = 4°$, $P = 1.9 \times 10^8$ years; in the outer regions, near $r = 8°$, $P \simeq 4.3 \times 10^8$ years. It is noteworthy that the whole length of the bar of the system is within the region of quasi-solid-body rotation ($r < 2°$).

IV. MASS

Kerr and de Vaucouleurs (1956) have discussed the mass derivation problem. The increased rotational velocities simplify the problem in one respect, namely, that the kinetic energy in the random motions is no longer a significant fraction of the rotational energy as the radio data suggested. On the other hand, the optical data reach hardly, if at all, beyond the velocity maximum and give no indication of the Keplerian branch of the rotation-curve, as the radio data did.[3] Further, the optical data are strongly unbalanced with only 7 objects on the south side of the minor axis, all within 2° from C, as against 16 objects on the north side, reaching to beyond 4° from the rotation center. Unfortunately, this is unavoidable, since the distribution of supergiant stars and emission nebulosities in the Cloud is asymmetrical with respect to the bar, with a heavy preponderance on its north side (Henize and Miller 1951, Fig. 3). This is a basic weakness of the optical approach. In addition, it is possible that the rotation-curve itself is asymmetrical; it will be recalled that, as noted in Section III, the radio observations were forced to fit a symmetrical curve by shifting the position of the adopted rotation center; this was necessary because the radio rotation curve was asymmetrical with respect to the optical center C and because there is at present no theoretical dynamical model with which such an asymmetrical curve could be interpreted.

In the present case the observations do not extend far enough on the south side to display asymmetry, if any, in the optical velocity curve; it is therefore possible to use the standard symmetrical models to discuss the optical rotation-curve, which, strictly speaking, applies only to the central regions and northern half of the Cloud.

The distance adopted here is $\Delta = 63$ kpc ($m_0 - M = 19.0$) as against 46 kpc in the 1955 discussion (de Vaucouleurs 1955*b*); the scale factor is $1° = 1.10$ kpc.

The Keplerian mass for the outer mean point $V_r = 143.5$ km/sec at $r = 4\overset{\circ}{.}02 = 4.42$ kpc is $\mathfrak{M}_0 = V^2 r/G = 2.1 \times 10^{10}\ \odot$; this, of course, is only a lower limit.

The Bottlinger formula leads to a very simple expression for the total mass (Lohman 1954):

$$\mathfrak{M}_B = \frac{a}{bG}. \tag{5}$$

Here $a = 2.73 \times 10^3$ (km/sec)^2 (kpc)$^{-2}$, $b = 0.018$ (kpc)$^{-3}$, and $\mathfrak{M}_B = 3.7 \times 10^{10}\ \odot$. The discussion of the radio data has shown that this formula probably gives an upper limit of the mass.

A closer approximation to the actual value can be derived from a model based on nonhomogeneous oblate spheroids (Perek 1948, 1950) in which the density law is of the form

$$\rho = \rho_c (1 - m^2), \tag{6}$$

where

$$m^2 = \frac{x^2 + y^2}{a^2} + \frac{z^2}{c^2}.$$

The rotational velocity is given by the equation for the central force in the equatorial plane,

$$\alpha a \rho_c = \beta = \frac{V_r^2}{r}, \tag{7}$$

where α is a numerical coefficient depending only on r/a for a given value of c/a. The values of α in Figure 4 computed by means of Perek's tables and nomograms are for $c/a = \frac{1}{5}$, a value selected by analogy with NGC 55 (Kerr and de Vaucouleurs 1956).

[3] The early discussions of a possible transverse effect should be kept in mind here; while a translation velocity of 600–700 km/sec is out of the question, a velocity of the order of 100 km/sec remains plausible, and there is nothing in the data to disprove it. In fact, a transverse velocity of only 50 km/sec, in the general direction of the south pole, i.e , opposite to that suggested by the Hertzsprung-type solutions, would almost exactly compensate the decrease in rotational velocity beyond $r \simeq 4°$, suggested by the radio data for the regions south of the center. It is clear that little weight can be attached to the Keplerian branch until the gradient of the rotation-velocity base line has been determined by 21-cm observations extending to great distances ($r > 10°$) north and south of the center.

The observations determine two mean points:

(I) $\bar{r} = 1^{\circ}86$ (range: 1.23–2.91), $\langle V_r \rangle = 100 \pm 10$: (p.e.), $W = 6.76$;

(II) $\bar{r} = 4^{\circ}02$ (range: 3.46–4.24), $\langle V_r \rangle = 144 \pm 10$: (p.e.), $W = 4.10$.

An exact fit is then given by a composite model of two such spheroids of radii a' and a'' and central densities ρ_c' and ρ_c''; since the two equations determine only the products $a'\rho_c'$ and $a''\rho_c''$, a' and a'' must be chosen more or less arbitrarily; plausible values are $a' = 4^{\circ} = 4.4$ kpc, corresponding roughly to the mean radius of the classical "main body," and $a'' = 8^{\circ} = 8.8$ kpc, corresponding to the mean radius of the faint outer regions detected on long-exposure photographs (de Vaucouleurs 1955*a*, 1957*a*). The results are collected in Table 4; the projected central density,

$$\sigma_c = 0.266 a \rho_c , \tag{8}$$

and total mass,

$$\mathfrak{M} = 0.335 a^3 \rho_c , \tag{9}$$

are also given.

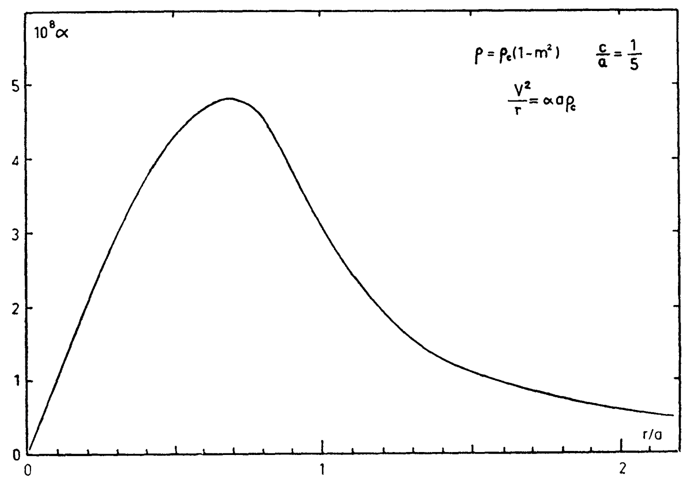

FIG. 4.—Coefficient α of the force-curve in the equatorial plane of an inhomogeneous oblate spheroid for the density law given by equation (6) and axial ratio $c/a = \frac{1}{5}$.

TABLE 4

ELEMENTS OF A COMPOSITE OBLATE SPHEROIDAL MODEL

Component	I	II	Total	Unit
a .	1 36	2 72	2 72	10^{22} cm
	4 4	8 8	8 8	kpc
ρ_c	23 6	4 42	28 0	10^{-24} gm cm^{-3}
	0 348	0 065	0 413	$\odot$/pc^3
σ_c	85 5	32	117	10^{-3} gm cm^{-2}
	410	153	563	$\odot$/pc^2
$\mathfrak{M}$.	19 9	29 6	49 5	10^{42} gm
	10 0	14 9	24 9	$10^9\odot$

The computed velocity-curve is shown by the continuous curve in Figure 3. The projected mass-density distribution, $\sigma_{\mathfrak{M}}(r)$, is shown in Figure 5 and tabulated in Table 6, third column; the fraction of the total mass within radius r from the center $(\mathfrak{M})_0^r$ is given in the fourth column; half the total mass of the model is within $r_e(\mathfrak{M}) = 2\overset{\circ}{.}9$ from the center. For comparison, the effective radius for red light is $r_e(\mathfrak{L}) = 2\overset{\circ}{.}6$ (de Vaucouleurs 1957*a*)[4] and for neutral hydrogen $r_e(\mathrm{H}) = 3\overset{\circ}{.}0$ (de Vaucouleurs 1957*b*). As expected, the total mass is intermediate between the lower and upper limits previously estimated; on present evidence the value

$$\mathfrak{M} = (2.5 \pm 0.6) \times 10^{10} \odot$$

may be adopted as the best optical estimate of the mass of the Large Cloud for $m_0 - M = 19.0$. The internal probable error is about 25 per cent, arising from the following sources:

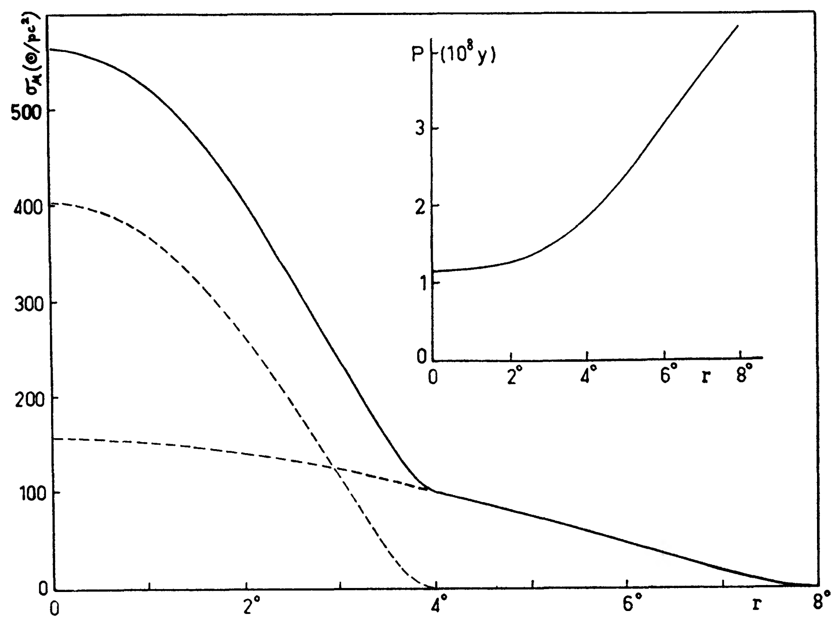

FIG. 5.—Projected density and rotation period of composite spheroid model. The density-curves of the two components are shown by the dashed lines

Velocities: $$\frac{\Delta\mathfrak{M}}{\mathfrak{M}} = \frac{2\Delta V_r}{V_r} = 2 \times \frac{10}{145} = 14 \text{ per cent},$$

Tilt: $$\frac{\Delta \sec^2 i}{\sec^2 i} = \frac{1.0}{5.0} = 20 \text{ per cent},$$

Model: $$\text{about } (\tfrac{1}{8}) \text{ total range} = \frac{1}{4} \cdot \frac{3.7 - 2.1}{3.7 + 2.1} = 7 \text{ per cent}.$$

V. MASS-LUMINOSITY RATIO

The integrated magnitudes of the Large Cloud out to $r = 8°$ or $A \simeq 200$ square degrees are $m = +0.30$ (V) and $+0.80$ (B) (Eggen and de Vaucouleurs 1956; de Vaucouleurs 1957*a*). The absolute magnitudes of the sun are $M = +4.84$ (V) and $+5.47$ (B)

[4] A more recent rediscussion of all available photometric data gives a revised value $r_e(\mathfrak{L}) = 3°0$ for red light and $r_e(\mathfrak{L}) = 2\overset{\circ}{.}9$ for blue light (de Vaucouleurs 1960)

(Stebbins and Kron 1957); the absolute luminosities and mass-luminosity ratios are listed in Table 5 for the apparent distance moduli $m - M = 19.15$ (V) and 19.2 (B) corresponding to $m_0 - M = 19.0$. The observed luminosities are listed in the first half of the table; values corrected for internal absorption in the system are given in the second half. According to Holmberg (1958), the total self-absorption in face-on, late-type spirals is 0.28 mag. (pg); the corresponding values for the tilt of the Large Cloud are 0.32 (B) and 0.24 (V). The absorption-free mass-luminosity ratio is about 6; very nearly the same value was derived recently for the flat component of M31 (de Vaucouleurs 1958) and for M33 (de Vaucouleurs 1959). It may be typical of large population I systems.

TABLE 5

MASS-LUMINOSITY RATIOS

	M	log $\mathfrak{L}$	$\mathfrak{M}/\mathfrak{L}$	M_0	log $\mathfrak{L}_0$	$\mathfrak{M}/\mathfrak{L}_0$
V	−18 85	9 475	8 4	−19 09	9 572	6 7
B	−18 40	9 55	7 1	−18 72	9 676	5 3

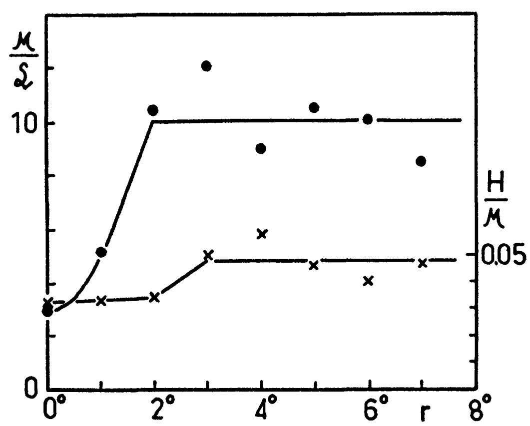

FIG 6 —Mass-luminosity ratio (*dots, left scale*) and hydrogen-to-total-mass ratio (*crosses, right scale*)

An indication of the possible variation of the mass-luminosity ratio with distance is given by Figure 6, showing the ratio of the surface mass density $\sigma_{\mathfrak{M}}$ according to the composite spheroid model to the average surface brightness $\sigma_{\mathfrak{L}}$ (V); the latter is derived from the integrated luminosity distribution in red light (de Vaucouleurs 1957*a*, Table X), corrected to visual light-units $V = R + (V - R) = 6.35 + 0.40 = 6.75$ mag/sq deg corresponding to 6.50 $\odot/\text{pc}^2$. The numerical values are listed in Table 6. $\mathfrak{M}/\mathfrak{L}$ is nearly constant for $r > 2^\circ$; the fluctuation near $r = 4^\circ$ reflects mainly the discontinuity in the model at the edge of the inner spheroid.

VI. RATIO OF NEUTRAL HYDROGEN TO TOTAL MASS

The integrated mass of neutral hydrogen within $\bar{r} = 7^\circ\!.3$ from the center, or in an area $A = 165$ square degrees, was previously estimated at 0.57×10^9 $\odot$ for $\Delta = 46$ kpc (Kerr and de Vaucouleurs 1956); at the revised distance $\Delta = 63$ kpc, this value is 1.07×10^9 $\odot$; thus we take $\mathfrak{M}(\text{H I}) = 1.1 \times 10^9$ $\odot$ within 200 square degrees. The corresponding ratio of neutral hydrogen to total mass, H I/$\mathfrak{M}$ = 4.4 per cent, is only a little larger than in M31, where it is about 1.5 per cent (van de Hulst *et al.* 1957), and in the

Galaxy, where it is about 2 per cent (Kerr and Hindman 1957); it is nearly the same as in M33, where it is 5.5 per cent (Volders 1959).

The ratio of the mean surface density of neutral hydrogen σ_H to the surface mass density $\sigma_{\mathfrak{M}}$ according to the model is given in Table 6 and in Figure 6. Except for the fluctuation near $r = 4°$, due mainly to the discontinuity in the model, the H I/$\mathfrak{M}$ ratio is almost constant. The values at $r \leq 1°$ are not significant, however, because of the large smoothing by the 1°5 beam (at half-power) of the radiotelescope. The data do not exclude the possibility of a strong concentration of neutral hydrogen in the bar.

Finally, it should be kept in mind that the hydrogen densities are only lower limits because of the neglect of self-absorption and of the unknown ionized fraction. In addition, the calibration of the 21-cm-line intensities has an uncertainty of about 20 per cent (Kerr *et al.* 1954).

TABLE 6

MASS, LUMINOSITY, AND NEUTRAL HYDROGEN DISTRIBUTIONS

r (°)	r (kpc)	$\sigma_{\mathfrak{M}}$ (⊙/pc²)	$(\mathfrak{M})_0^r$	$\sigma_{\mathfrak{L}}(V)$ (⊙/pc²)	$(\mathfrak{L})_0^r$	σ_H (⊙/pc²)	$(H)_0^r$	$\mathfrak{M}/\mathfrak{L}_v$	H/$\mathfrak{M}$
0	0 0	563	0	(195)	0	(18 2)	0	(2 9)	(0 032)
1	1 1	524	0 081	103	0 178	17 0	0 06	5 1	033
2	2 2	405	0 290	39	0 423	13 8	22	10 4	034
3	3 3	241	0 532	20	0 602	11 9	45	12 0	050
4	4 4	99	0 709	11	0 733	5 8	67	9 0	058
5	5 5	73	0 825	7	0 835	3 4	81	10 5	046
6	6 6	45	0 922	4 5	0 911	1 8	92	10:	040
7	7 7	17	0 983	2 0:	0 967	0 8:	0 97	8 5:	0 047:
8	8 8	0	1	(0)		(0)			
Σ(⊙ =1)			25×10⁹		3 0×10⁹		1 1×10⁹	8 4	0 044
r_e			2°9		2°6		3°0*		

* Corrected for beam smoothing

VII. COMBINED MASS OF THE CLOUDS

The mass of the Small Cloud is probably between one-fifth and one-half the mass of the Large Cloud (Kerr and de Vaucouleurs 1956) or 5–15 $\times 10^9$ ⊙; the total mass of the pair is then between 3 and 4 $\times 10^{10}$ ⊙.

The differential radial velocity between the Large and the Small Cloud is 50–60 km/sec; the projected separation of the centers is 23 kpc on the revised distance scale. The radio observations suggested that the total mass of the pair was too small to establish a closed orbit; the new results reverse this conclusion. For a parabolic orbit the minimum mass is 10^{10} solar masses; for a circular orbit, 2×10^{10} solar masses. Unless the tilt of the orbital plane to the line of sight is large, a closed orbit is possible.

There is also a distinct possibility that the Clouds form with the Galaxy a stable triple system, especially in view of the fact that the residual radial velocity of the center of gravity of the two Clouds is close to zero. With present estimates of the combined mass of the Clouds, say $\mathfrak{M}_c = 3.5 \times 10^{10}$ ⊙, and of the Galaxy, $\mathfrak{M}_G = 7 \times 10^{10}$ ⊙ (Schmidt 1956), the center of gravity of the triplet is located about 20 kpc from the galactic center in galactocentric longitude $l' = 278°$ (sun at $l' = 180°$), latitude $b' = -38°$. For a circular orbit the period of revolution is $P = 4.3 \times 10^9$ years, the orbital velocity of the Galaxy is $v_0 = 28.4$ km/sec, that of the center of gravity of the Clouds is $2v_0 = 56.8$

km/sec. As noted in Section IV, a transverse velocity of this order could greatly change the apparent slope of the outer parts of the radio rotation-curve of the Large Cloud.

The increased estimates of the masses of the Clouds reduce greatly the role of perturbations by the Galaxy; with the values above, the tidal force $\propto \mathfrak{M}/\Delta^3$ at the Small Cloud is only about 15 per cent of that caused by the Large Cloud; this makes it easier to understand why the prominence of the Small Cloud points directly toward the Large Cloud. On the other hand, the tidal forces exerted by the Small Cloud and by the Galaxy on the Large Cloud are more nearly equal.

The large combined mass of the Magellanic Clouds may also help to explain the distortion of the outer regions of the galactic "plane" (Kerr *et al.* 1957). An early estimate of the expected tidal distortion based on the radio data (Kerr 1957) suggested a discrepancy of two orders of magnitude. With the new values, the tidal force accounts for a fraction of the observed effect, which is about one-tenth away from the Clouds and one-third toward the Clouds; thus, while purely gravitational effects do not seem to explain the whole distortion, they may contribute significantly to it if the present mass estimates are accepted. However, in view of the much smaller mass previously derived from the radio data, this conclusion can be regarded as only tentative and the mass values subject to revision after comparison with new radio observations now being planned at Sydney. The present situation is reviewed in Appendix II.

The spectral observations with the 74-inch reflector were made by permission of Dr. A. R. Hogg, then Acting Commonwealth Astronomer, under the co-operative arrangement between the Commonwealth Observatory and the Yale-Columbia Southern Station. The assistance rendered by several members of the observatory staff in the early period of operation of the telescope and spectrograph is gratefully acknowledged, and so is the collaboration of Mrs. A. de Vaucouleurs, who performed most of the measurements and reductions of the plates. I am indebted to Mr. F. J. Kerr for valuable comments on the first draft of the manuscript.

APPENDIX I

On the Spiral Structure of the Large Cloud

Because of the traditional classification of the Magellanic Clouds as "irregular" galaxies, the reality of the spiral structure observed in them at Mount Stromlo is still often questioned. The following remarks may help to clarify this point.

The presence of spiral structure was first detected by star counts (de Vaucouleurs 1954*a*); it was, however, much confused by foreground stars, and subsequent photographic observations (de Vaucouleurs 1954*b*, 1955*a*) did not confirm in detail the complex spiral pattern as initially sketched. The photographs showed, instead, that wo types of spiral-like structure are present: (1) in the bright, inner regions of diameter $6^\circ \times 7^\circ$, short, irregular, or elongated star clouds and fragmentary spiral arcs first noticed many years ago by H. C. Russell (1890) and more recently by Shapley (1951); (2) in the faint, outer regions of diameter $10^\circ \times 11^\circ$, a long, broad, and regular loop which sweeps around the "main body" from north, near 5^h10, -64°, to east, near 6^h10, -70°, to south, near 5^h30, -74°, as indicated by the outline sketch in Figure 1.

These two sections of the structure merge smoothly into each other and are obviously parts of the same over-all spiral pattern, as can be clearly seen on the mosaic photograph and key map published earlier (de Vaucouleurs 1954*b*, 1955*a*). Although this loop shows up on all long-exposure plates taken with a variety of cameras at Mount Stromlo, it is difficult to print satisfactorily because of its faintness, its large angular size, and the crowded star field. The prints of different densities in Figure 7 should help to identify it by comparison with Figure 1. The classical "main body" can be recognized on the lighter print; it is completely black on the denser prints. The emission nebulosities observed for radial velocity are all in this central region. In addition, faint outlying filaments, definitely real but of uncertain nature, extend the structure beyond the region of immediate interest for rotation studies.

If the outer loop was not detected sooner in the Large Cloud, it is probably not only because

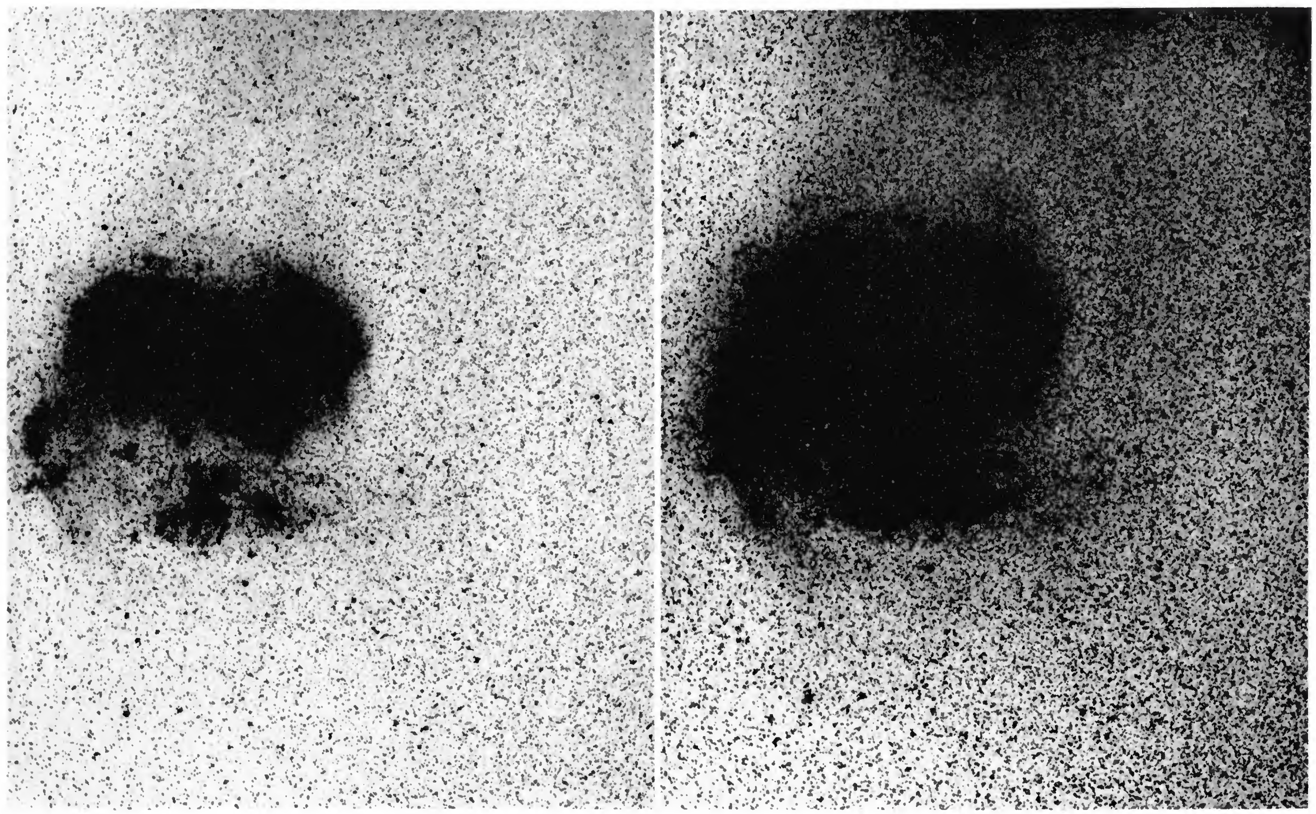

FIG. 7.—Spiral structure in the Large Magellanic Cloud. 7-inch, $f/4$ Aero-Ektar photographs, 103a-O, exposure 1 hour, Mount Stromlo, 1954.

it is large and faint but also because it lacks the bright blue supergiants and emission knots which make the inner branches so conspicuous; the stellar population in this outer arm is probably similar to that in the south-preceding wing of the Small Cloud, which is resolved only at magnitude $m > 14.5$, beyond which stars appear suddenly in large numbers. The differences between luminosity functions in different parts of the Magellanic Clouds have been previously discussed (de Vaucouleurs 1956). Another characteristic of the outer arm is that it is poor in interstellar hydrogen (de Vaucouleurs 1957*b*) a fact that correlates well with the population characteristics.

APPENDIX II

Radio and Optical Rotation Velocities

The 21-cm-line profiles show a complex structure with several peaks and a total width of 70–90 km/sec in the central regions of the Cloud.[5] In the outer parts the line shows pronounced skewness and a total width of 50–70 km/sec.

The initial rotational analysis (Kerr and de Vaucouleurs 1955) was based on the median velocities, i.e , the velocities halving the area under the line profile; however, comparison with the Lick optical velocities of emission nebulosities showed immediately that this median velocity does not refer to the equatorial plane of the system (*ibid.*, Fig. 6). It was then found that the peak velocities, i.e., the velocities at the main peaks of the line profiles, are everywhere greater than the median velocities and are consistent with the optical velocities within 2° from the center. The mass was therefore derived from an analysis of the rotation-curve given by the peak velocities, roughly corrected for the smoothing effect of the finite beam width (1°.5) of the radio-telescope. This analysis gave $\mathfrak{M} = 3 \times 10^9 \odot$ for $i = 65°$ and $\Delta = 46$ kpc. The present value $\mathfrak{M} = 25 \times 10^9 \odot$ is 8.3 times larger, of which a factor $\times 1.37$ is due merely to a change in distance scale and a factor $\times 6.0$ due to the higher rotational velocities indicated by the optical observations.

It is important to determine whether this discrepancy corresponding to a factor $\sqrt{6} = 2.45$ in the velocities is real or merely due to uncertainties in the observations or their reduction. A discrepancy between radio peak velocity and optical velocity was already apparent in the Lick data, which gave a rotational velocity 30–40 per cent larger than the radio peak velocities near $r = 3°–4°$ (*ibid.* Fig. 6), but the absolute difference in the line-of-sight component (10–15 km/sec) was not much in excess of the combined uncertainty of the data then available, and it was ignored. The new Mount Stromlo data, however, confirm the Lick data and, if anything, increase rather than decrease the discrepancy with the radio data.

In order to avoid as far as possible any question of choice of a rotation center (cf. Sec. III*a*) and because the optical observations extend hardly beyond the maximum of the rotation-curve, it is indicated to base the discussion on the slope of the quasi-linear branch of the rotation-curve. Along the major axis in p.a. 165° this straight part extends over some 6° from about 2° south of the bar to about 4° north of it. As noted before, the velocity gradient along this direction is practically independent of the value assumed for the galactic rotation correction (Sec. III*d*). The comparison is shown in Table 7.

The close agreement between the two completely independent optical determinations (12 H II regions observed at Lick and Mount Stromlo, 26 supergiant stars observed at Pretoria) leaves little doubt that their results are significant, and, because of the nature of the objects observed, they refer to the equatorial plane of the system. It must be concluded that even the peak radio velocities do not originate in this plane but refer to some unknown mean height above and below the plane where rotational velocities are smaller. The alternative that the gas is in the equatorial plane but rotates more slowly than the stars cannot be positively excluded at present; it does not appear very attractive, however, especially since the width of the 21-cm-line profiles tends to support the idea of a widespread z distribution of H I.

The z density distribution at distance r from the center may be written $\rho_H(r, z) = \rho_H(r, 0)\psi(z)$, where $0 \leq \psi(z) \leq 1$ decreases as $|z|$ increases. The mean height $\langle z \rangle$ of the gas is given by $\psi\langle z \rangle = 0.5 \int_0^\infty \psi(z)dz$; i e., half the total mass of gas will be within $\pm \langle z \rangle$ from the equatorial plane Simi-

[5] See Fig 7 in the paper by Kerr and the writer (1955), where the scale of velocities should read 230–330 km/sec, not 130–230 km/sec.

larly, the rotational velocity is $V_r(z) = V_r(0)\phi(z)$, where $0 \leq \phi(z) \leq 1$ decreases as $|z|$ increases. The mass of gas along any line of sight with rotational velocity between V_r and $V_r + dV_r$, i.e., the monochromatic flux in the 21-cm line, is determined by the density and velocity distributions and by the velocity dispersion σ_V.

An exact computation is not yet possible, but for a rough estimate let us neglect σ_V and assume that $\psi(z) = \exp(-z^2/\zeta^2)$ and $\phi(z) = \exp(-z^2/\tau^2)$, with $\zeta = 1.5$ kpc and $\tau = 1$ kpc, then $\langle z \rangle = 0.67 \ldots \zeta = 1$ kpc and $\phi(\langle z \rangle) = e^{-1} = 0.434$. If the gradient along the major axis of the line-of-sight component of the equatorial rotational velocity is $G(0) = dV_r(0) \cos i/dx = 16$ km/sec, as indicated by the optical data in Table 7, then at $\langle z \rangle$ it is $G(1) = 7$ km/sec in approximate agreement with the radio median velocity. Since, in general, ψ and ϕ may also be functions of r and the gas in the corona may very well have, in addition, a z velocity component $V_z(r, z)$, it is evident that the actual physical situation may be very complicated and no simple interpretation of the line profiles is possible at present; in particular, it is not possible to identify with any degree of certainty the velocity that arises from the equatorial gas layer in the broad-line profile. All that can be said is that this velocity must be greater than the peak velocity on the north side of the minor axis and smaller south of it. In other words, it must be located on the steeper wing of the asymmetrical line profile.

TABLE 7

MEAN GRADIENT (KM/SEC PER DEGREE) ALONG MAJOR AXIS OF LINE-OF-SIGHT COMPONENT OF ROTATION VELOCITY

Velocity	Gradient	Source
Radio median H I	6 0	1
Radio peak H I . .	9 3	2
Optical, 12 H II regions	16 9	3
Optical, 26 supergiant stars	16 0	4

NOTES TO TABLE 7

1. Kerr and de Vaucouleurs (1955, Figs. 2 and 3).
2. *Ibid.*, Fig. 6.
3. Section III*e* for $V_S = +10$ with $\langle f \rangle = 2$ 65.
4. Feast, Thackeray, and Wesselink (1955).

An inspection of typical line profiles (Kerr and de Vaucouleurs 1955, Fig. 6) shows that this interpretation is consistent with the observed line widths. It follows that the main cause of line broadening is not a random velocity dispersion of some 20–25 km/sec, as assumed in the initial analysis, but primarily the rotational-velocity gradient along the line of sight in an extended corona. In addition to this first effect, if the velocity-curve is actually asymmetrical with respect to C, as suggested by the radio data, the rotational velocities being larger on the north side, the mass derived from optical velocities of objects predominantly located north of the center (4° N. to 2° S.) is bound to be higher than the mass derived from the radio velocities, which give a more complete coverage, especially to the south (6° N. to 11° S.). The maximum radio median velocities are +25 km/sec about 4° north of C, −10 km/sec about 2° south of C (*ibid.*, Fig. 2*b*); it follows that if the optical velocities at $z \simeq 0$ are everywhere simply proportional to the radio median velocities at $z = \langle z \rangle$, the rotational velocities for the north side will be about $25/17.5 = 1.43$ times greater than mean velocities of both sides at the same r. This is very nearly the factor required to account for the remaining discrepancy between the radio and optical results, as shown below:

1. Rotational velocity gradient between $z = 0$ and $\langle z \rangle_{\mathrm{H}}$	×1 82
2. North-south asymmetry of velocity-curve .	×1 43
Total	×2 60
Observed . . .	×2 45

If this interpretation is substantially correct, the mass derived from the radio data is too low because of the $\langle z\rangle$ effect 1; the corrected value, reduced to $\mathfrak{M} = 63$ kpc, then, is

$$\mathfrak{M}_1 = 1.37 \times (1.82)^2 \times 3 \times 10^9 = 14 \times 10^9 \odot \; .$$

The mass derived from the optical data is too high because of the asymmetry effect 2, the corrected value is

$$\mathfrak{M}_2 = (1.43)^{-2} \times 25 \times 10^9 = 12 \times 10^9 \odot \; .$$

New radio observations with improved resolution and sensitivity and additional optical velocities of stars and nebulae over as wide an area as possible are needed for a more detailed discussion, but it might be concluded that on present evidence the most probable estimate of the mass of the Large Cloud is $\mathfrak{M} = (1.3 \pm 0.3) \times 10^{10}$ solar masses if $\Delta = 63$ kpc; then $\mathfrak{M}/\mathfrak{L} \simeq 4 \pm 1$ and H I$/\mathfrak{M} \simeq (9 \pm 2) \times 10^{-2}$.

A combined analysis of both optical and radio data should then lead to a better understanding of the complex velocity field of stellar and interstellar matter in the Magellanic Clouds. In addition, attempts should be made to explore the dynamics of non-stationary, asymmetrical models with non-axisymmetric velocity fields, which may prove necessary for a correct interpretation of the observed velocity distribution.

REFERENCES

Eggen, O. J., and Vaucouleurs, G. de. 1956, *Pub. A.S P* , **68**, 421.
Feast, M. W., Thackeray, A. D., and Wesselink, A. J. 1955, *Observatory*, **75**, 216
Henize, K. G. 1956, *Ap. J. Suppl.*, **2**, No 22, 315.
Henize, K. G., and Miller, F. D. 1951, *Pub. Obs. U. Michigan*, **10**, 75
Hertzsprung, E. 1920, *M.N* , **80**, 782.
———. 1923, *ibid.*, **83**, 348.
Holmberg, E. 1958, *Medd. Lunds Obs.*, Ser. II, No. 136.
Hulst, H. C. van de, *et al.* 1957, *B.A N.*, **14**, 14 (No. 480).
Humason, M. L., and Wahlquist, H. 1955, *A.J.*, **60**, 254.
Kaburaki, M. 1931, *Proc. Phys -Math. Soc Japan*, **13**, 151.
Kerr, F. J. 1957, *A.J* , **62**, 93.
Kerr, F. J., and Hindman, J. V. 1957, *Pub. A.S.P.*, **69**, 558.
Kerr, F. J., Hindman, J. V., and Robinson, B. J. 1954, *Australian J. Phys* , **7**, 297.
Kerr, F. J , Hindman, J. V , and Stahr Carpenter, M. 1957, *Nature*, **180**, 677.
Kerr, F. J., and Vaucouleurs, G. de. 1955, *Australian J. Phys.*, **8**, 508.
———. 1956, *ibid.*, **9**, 90
Lohmann, W. 1954, *Z. f. Ap.*, **35**, 159
Luyten, W. J. 1928, *Proc. Nat. Acad Sci* , **14**, 241 (H. Rep. 44)
Perek, L. 1948, *Contr. Astr. Inst. Masaryk U.*, Vol. **1**, No. 6
———. 1950, *Bull. Astr. Inst. Czechoslovakia*, **2**, 75
Russell, H. C. 1890, *M.N.*, **51**, 41 and 96.
Schmidt, M. 1956, *B.A N.*, **13**, 15 (No. 468).
Shapley, H. 1951, *Pub. Obs. U. Michigan*, **10**, 79.
Stebbins, J , and Kron, G. E. 1957, *Ap. J.*, **126**, 266
Vaucouleurs, G. de 1954*a*, *Observatory*, **74**, 23.
——— 1954*b*, *ibid* , p. 158.
——— 1955*a*, *A.J* , **60**, 126.
——— 1955*b*, *Pub. A.S P* , **67**, 350
———. 1955*c*, *ibid.*, p. 397
——— 1956, *Irish A.J.*, **4**, 13.
——— 1957*a*, *A.J.*, **62**, 69.
———. 1957*b*, *I A U. Symposium*, No 4: *Radio Astronomy*, p 244
———. 1958, *Ap. J.*, **128**, 485
——— 1959, *ibid.*, **130**, 728.
——— 1960, *ibid.* (in press).
Vaucouleurs, G. de, and Vaucouleurs, A. de 1960, *Mem. R A S* , in press.
Volders, L. 1959, *Bull. Astr Inst Netherlands*, **14**, 323
Voute, J. 1926, *Ann. Bosscha-Sterr Lembang*, Vol **3**.
Wilson, R E. 1918, *Pub. Lick Obs* , **13**, Part 5, 187.
———. 1944, *Pub A S P* , **56**, 102, 203.